Research Article | Vol. 27, No. 20 | 30 Sep 2019 | OPTICS EXPRESS 28722
Optics EXPRESS

Conformal optical devices based on geodesic lenses

LIN XU,[1] TOMÁŠ TYC,[2] AND HUANYANG CHEN[3,*]

[1]*Key Laboratory of Opto-Electronic Information Acquisition and Manipulation of Ministry of Education, Institutes of Physical Science and Information Technology, Anhui University, Hefei 230601, China*
[2]*Department of Theoretical Physics and Astrophysics, Masaryk University, Kotlarska 2, 61137 Brno, Czech Republic*
[3]*Institute of Electromagnetics and Acoustics and Key Laboratory of Electromagnetic Wave Science and Detection Technology, Xiamen University, Xiamen 361005, China*
[*]*kenyon@xmu.edu.cn*

Abstract: Conformal transformation optics provides a simple scheme for manipulating light rays with inhomogeneous isotropic dielectrics. However, there is usually discontinuity for refractive index profile at branch cuts of different virtual Riemann sheets, hence compromising the functionalities. To deal with that, we present a special method for conformal transformation optics based on geodesic lenses with special closed surfaces. The requirement is a continuous refractive index profile of dielectrics, which shows the almost perfect performance of designed devices. We demonstrate such a proposal by achieving conformal transparency (invisibility without cloaking region) and reflection. We can further achieve conformal invisible cloaks by two methods with perfect conductors. The conformal transformation optics method based on geodesic lenses may also find applications in other waves that obey the Helmholtz wave equation in two dimensions.

1. Introduction

Based on the form invariance of Maxwell's equations and multi-linear electromagnetic constitutive equations, the optical property of virtual space and physical space could be connected by a coordinate mapping [1]. In 2006, Leonhardt [2] presented that a conformal coordinate mapping between two complex planes could be performed for the scalar field of the refractive index of dielectrics such that light rays could be manipulated freely. Coincidentally, Pendry et al [3] provided a general method for controlling the electromagnetic field in space of three dimensions. These two seminal papers launched a new research field named transformation optics (TO) [4–7], which mainly focused on optical invisibility. After that, a lot of optical designs based on TO were proposed, such as carpet cloak [8], illusion optics devices [9], field rotator [10] and so on. With the development of metamaterials, several proof-of-principle experiments have been achieved, like the reduced cloak in two dimensions [11], carpet cloaks [12,13], field rotator [14] and concentrator [15]. Besides metamaterials, structured materials like photonic crystals [16] and waveguides [17], could also serve for designing transformation materials, which provide different platforms. More recently, the optical cavities in visible region based on TO have attracted a lot of attention, such as mimicking the gravitational lens [18] and Einstein's ring [19]. In addition, the idea of TO has also been extended to other waves, such as acoustics [20], plasmonics [21] and thermodynamics [22].

From the geometrical perspective, TO has been established for the connection between curved space-time and the multi-linear electromagnetic response of structured materials, which gives a blueprint to control light propagation. Despite these versatile design proposals and proof-of-principle experiments, TO still encounter challenges in practical engineering because of the complexity of the required materials. Take the design of invisibility for

#371956 https://doi.org/10.1364/OE.27.028722
Journal © 2019 Received 11 Jul 2019; revised 3 Sep 2019; accepted 4 Sep 2019; published 23 Sep 2019

Optics EXPRESS

example, the required tensor fields of permittivity and permeability have infinity values at some points [3]. At the same time, conformal transformation optics (CTO) (in two-dimensional space) was proposed by Leonhardt [2] as a simpler scheme for manipulating light rays by using dielectrics with inhomogeneous isotropic refractive index profile, which is a scalar field. After that, lots of designs with CTO have been proposed, like conformal invisible cloaks [23–25], conformal transparency devices [26], conformal illusion devices [27] and conformal Talbot devices [28]. Recently, some interesting devices are proposed by merging geometric optical design with CTO, such as bidirectional focusing [29]. Though some experiments [28,30,31] have also demonstrated the principle of CTO [2,32], there is still a need to optimize the design procedure, so that a feasible scalar field of refractive index can be obtained for practical applications. Moreover, in several proposals of CTO [2,24,25], there is a discontinuity of refractive index profile along the branch cut of the conformal mapping, which might have some unwanted influence on the performance of CTO in turn.

In this paper, to solve the problems caused by discontinuity of refractive index profile, we propose a special kind of CTO based on geodesic lenses [33–36]. The mapping of such method is a composite mapping of the geodesic mapping and the analytical conformal mapping, which could map an artificial Riemann surface (virtual space) with homogeneous refractive index profile to a plane (physical space) with inhomogeneous refractive index profile. The requirement of inhomogeneous refractive index is a continuous scalar field. We demonstrate our method by achieving optical transparency and wave reflection. To obtain invisible cloaks, we develop two methods with perfect electric conductors (PECs). Moreover, we explain that our method can work not only in the geometric-optical limit but also be extended to wave regime at a discrete series of frequencies.

2. Analytical conformal mapping and geodesic mapping

In traditional conformal transformation optics, we usually use analytical function $w = f(z)$ to connect complex plane z (physical space) with complex plane w (virtual space). This analytical conformal mapping (ACM) preserves the angle of two intersecting lines because of Cauchy-Riemann conditions [37]. The refractive index profiles of two complex planes have the relation based on CTO [2,32], which is written as

$$n(z) = \left|dw/dz\right| n'(w). \tag{1}$$

In general, two-dimensional surfaces are all conformally flat (angle preserved, not the length, after a conformal mapping) and they differ by a curvature scalar field [38]. For light rays, such a curvature scalar field could be treated as the scalar field of refractive index profile. Hence light rays follow the geodesic equation of that surface. There is a kind of coordinate transformation from an inhomogeneous plane lens with rotationally symmetric refractive index profile $n(r)$ to a surface of revolution with homogeneous refractive index profile $n'(h) = 1$ written as

$$\rho = n(r)r \text{ and } dh = n(r)dr, \tag{2}$$

where ρ is the radial coordinate, and h is the length measured along the meridian from North pole in the surface of revolution, as shown with examples in the left column of Fig. 1. The radial coordinate of the plane in the right column of Fig. 1 is denoted by r. And the azimuthal angle coordinate φ is not changed under Eq. (2). In this paper, apart from the numerical simulation results, all other figures are plotted with the commercial software Mathematica according to the geometry. Light rays propagate along geodesics of the surfaces, which are the shortest optical paths. Therefore, the surface of revolution is usually called a geodesic lens [36]. Here we use geodesic mapping (GM) to denote the mapping of Eq. (2), which is different from ACM. GM can preserve the angle of two intersecting lines in the

Optics EXPRESS

curved surface when it is mapped to that in the plane. Moreover, the optical path will not change, namely, $dh^2+\rho^2 d\varphi^2 = n^2(dr^2+r^2 d\varphi^2)$ according to Eq. (2), which sets up the equivalence of the corresponding optical path elements [33,36]. GM was also used to deal with three-dimensional Luneburg inverse problem associated with spherical media [33,34].

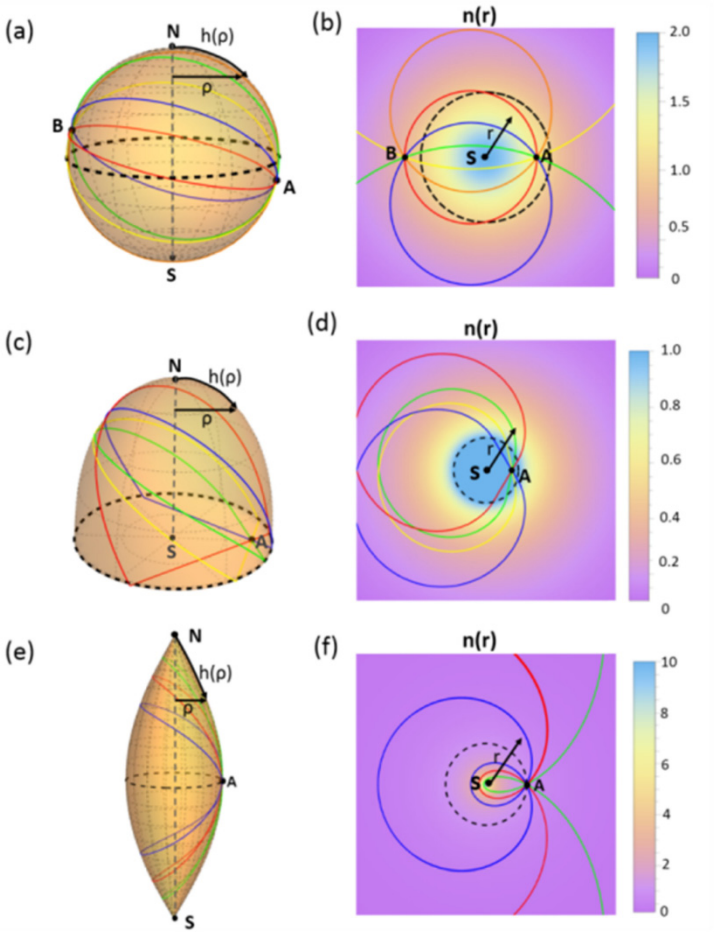

Fig. 1. Geodesic lenses (left column) and corresponding plane lens with rotational symmetry (right column). In geodesic lenses, the rotational symmetrical axis is the line which connects the North (N) pole and the South (S) pole. ρ is the radial coordinate, and $h(\rho)$ is the length measured along the meridian from N pole in the geodesic surface. Light rays starting from point A form closed trajectories shown in different colors. Those geodesic lenses are a sphere (a), truncated Tannery's pear (c) and spindle (e). Their descriptions are shown in Table 1. Their corresponding inhomogeneous plane lenses are Maxwell's fish-eye lens (b), inverse invisible lens (d) and generalized Maxwell's fish-eye (f), respectively. Contour plots show refractive index profile of $n(r)$ with rotational symmetry. Point S represents the origin of the plane, which mapped from S pole of geodesic lenses. The infinity corresponds to N pole. Colored light rays are mapped from those of geodesic lenses. Dashed black lines are places with the refractive index of unity at the radius of r_0 .

Optics EXPRESS

Table 1. Refractive index profiles of three absolute instruments and spectrum of the corresponding geodesic lens [a]

Refractive index profile	Geodesic lens	Description of geodesic lens	Spectrum
Maxwell's fish-eye lens			
$n(r)=\frac{2}{1+(r/r_0)^2}$	Sphere	$h(\rho)=\arcsin(\rho)$	$\omega r_0/c=\sqrt{(N+m)(N+m+1)}$ $\approx N+m+0.5,$
Inverse invisible lens			
$r>r_0,(r/r_0)n^{3/2}+(r/r_0)n^{1/2}=2;$ $r<r_0,n=1\ \ r<r_0,n=1;$	Truncated Tannery's pear	$h_1(\rho)=-\rho+2\arcsin(\rho);$ $h_2(\rho)=2+\pi-\rho$	$\omega r_0/c\approx N+m+0.5,$
Generalized Maxwell's fish-eye lens			
$n(r)=\frac{2(r/r_0)^{1/M-1}}{1+(r/r_0)^{2/M}},$ $M=2,3,4...$	Spindle	$h(\rho)=\arcsin(M\rho),$ $M=2,3,4...$	$\omega r_0/c=\sqrt{(N+M\cdot m)(N+M\cdot m+1)}/M$ $\approx (N+0.5)/M+m,$

[a]This spectrum is calculated by the numeric method in [39]. N determines the number of zeros of eigen-functions in the latitude direction, while m determines the phase change (in multiples of 2π) when encircling the geodesic lens along a latitude line.

For the sake of later discussion, we list three typical geodesic lenses (sphere, truncated Tannery's pear and spindle) and the corresponding inhomogeneous plane lenses (Maxwell's fish-eye lens, inverse invisible lens and Generalized Maxwell's fish-eye lens) with their properties summarized in Table 1 (for details, see in [39]). Tannery's pear is a two-dimensional compact surface and its geodesics are closed [40]. It turns out that geodesics of truncated Tannery's pear are also closed [34,39]. The spindle is equivalent to a portion of 1/M of a sphere, which is glued along its boundary [33,34,39,41]. All light rays form closed trajectories in these geodesic lenses and the corresponding plane lenses as shown in Fig. 1. Moreover, these three plane lenses are also called absolute instruments, where closed light rays and perfect imaging could be achieved [33,42]. We will use these geodesic lenses for further work in the following sections. In the wave regime, these geodesic lenses and plane lenses have the spectrum shown in the last column of Table 1. It turns out that their spectra are highly degenerated [39]. This is vital for the wave performance of our design.

3. Conformal transparency with geodesic lens

Transformation optics shows us a heuristic method to understand the certain complex medium as curved space for light [38]. Therefore, we usually start from a simple space, namely flat Euclidean space, to design the transformation medium to achieve a certain property, like invisible cloak [3]. Sometimes, we could also start from a non-Euclidean space to make an optical design with a fancy functionality [43]. Similarly, by compositing a GM and an ACM, we could achieve a mapping from virtual non-Euclidean space with homogeneous refractive index profile to a plane physical space with an inhomogeneous refractive index profile. Hence, we can design optical devices with an inhomogeneous refractive index profile in two dimensions by using such a composite conformal mapping. It gives geometric intuition for us to deal with problems in virtual space embedding in three dimensions, rather than in physical space plane with a complicated scalar field.

Let us start from a concrete example of conformal transparency to illustrate our method. Suppose that we have a non-Euclidean virtual space with a sphere and a meshed plane in Fig. 2(a). The radius of the sphere is R. They are connected by a branch cut (a solid arc in purple). For light rays in the plane, they travel along straight lines. When parallel light rays shown in different colors propagate in the plane and meet the branch cut, they enter a sphere and form closed trajectories of great circles, which are geodesics on the sphere. After they come back to the branch cut again on the sphere, they return to the plane to continue their journey with their positions and directions preserved. Compared with parallel light rays not entering into

Optics EXPRESS

the sphere, they have an additional optical path on the sphere. But for observers far away, this sphere appears invisible in the limit of geometrical optics.

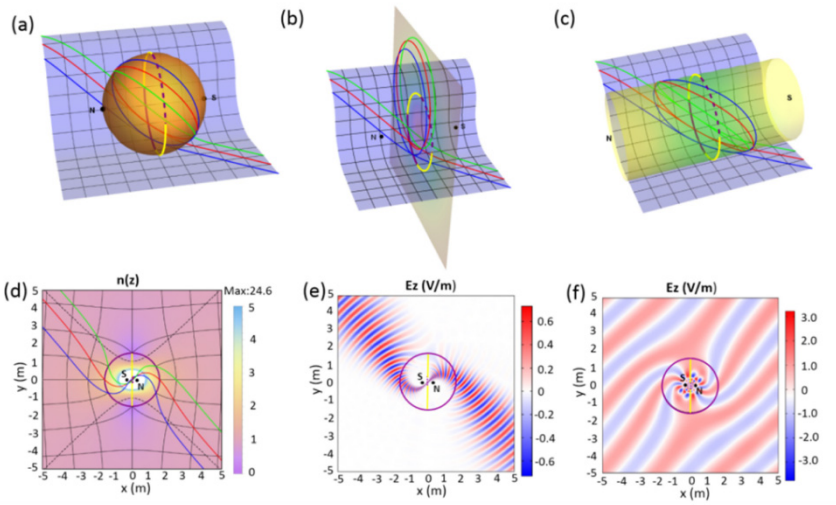

Fig. 2. Conformal transparency design based on a sphere. Virtual space (a) consists of a complex plane and a sphere. They are sewed along with a branch cut (solid arc in purple), which belongs to geodesics of both parts, namely a straight line in the plane and a great circle in the sphere. Dashed arc in purple is the image of the branch cut. The colored light rays are paralleled in plane and form closed trajectories in the sphere. Light rays started from the branch cut cannot reach two yellow arcs. N and S denote the poles of the sphere. Using geodesic mapping, the sphere in (a) is mapped to Maxwell's fish-eye lens (the vertical plane) in (b). The corresponding light rays also form closed trajectories. With a further exponential conformal mapping, Maxwell's fish-eye lens in (b) is mapped to a cylindrical Mikealian lens shown in (c). Therefore by using an analytical conformal mapping, final physical space is obtained in (d), with contour plot of refractive index profile (dashed black lines are places with the refractive index of unity). Corresponding light rays are shown in colored curves in (a-d). Gaussian beam in (e) and plane wave in (f) impinge our design at the angle of $-\pi/4$ at an eigenfrequency corresponding to $N+m=40$ and $N+m=10$, respectively. Here we set the radius of the sphere to be R = 2 and the length of the branch cut to be a quarter of a great circle for the illustration. The corresponding parameter a in an analytical conformal mapping is 0.3125.

After introducing a virtual space in Fig. 2(a), we perform a GM (written as Eq. (2)) of the sphere to obtain Maxwell's fish-eye lens shown in the vertical plane in Fig. 2(b), which still connect the original plane along with the branch cut. The exponential mapping is an analytical function, which can map a plane to a ribbon region. Moreover, the ribbon region can be treated as a cylinder. Hence, we further obtain a cylindrical Mikealian lens with a period of 8π shown in Fig. 2(c) by using $w_2 = \exp(w_1)$ of Maxwell's fish-eye lens [28]. Finally, we could map the whole space of Fig. 2(c) to physical space by an analytical conformal mapping, namely, $w_1 = z + 4\log(z-a) - 4\log(z+a)$ [25], which results in a continuous refractive index profile shown in contour plot of Fig. 2(d). The analytical conformal mapping is carefully chosen such that the branch cut is a quarter of a great circle in virtual space. Correspondingly light rays are shown in colored curves in Figs. 2(a)–2(d). So far, we have achieved conformal optical transparency based on a sphere, where the mapping is a composition of one geodesic mapping and two analytical conformal mappings. However, these mappings are carefully chosen such that virtual space and physical space are matched very well. Note that this profile is similar to that in [26], however, the current interpretation is more intrinsic in geometric perspective, hence will induce several designs in the following sections.

Optics EXPRESS

4. Performance in wave-optical regime

It turns out that conformal transformation optics not only work in geometrical optics but also at eigenfrequencies in wave regime [32,44]. Hence, light wave will accumulate multiple integer times of 2π when it is in the geodesic lens. Only at those eigenfrequencies can our conformal optical devices work. Since CTO connects the virtual space and physical space, we can analyze problems in simpler virtual space instead of physical space with the complex medium. As shown in Table 1, the frequency spectrum of Helmholtz equation in sphere is $\omega r_0 / c = \sqrt{(N+m)(N+m+1)} \approx N+m+0.5,$ where the number m is an integer that expresses the dependence of the eigenmode on the azimuthal angle φ as $\exp(im\varphi)$, and N is a non-negative integer expressing the number of nodes of the wave along the meridian between North and South poles. More details about spectrum could be found in [39, 45]. It means that light wave impinges in virtual space forms standing wave at those frequencies. As has been shown previously for related devices [46–48], there is almost perfect invisibility at the resonant frequencies of the non-Euclidean part of virtual space. For our case, this means illuminating the device by wave with a frequency corresponding to an integer $l = N+m$. To test this with our design, we set r_0=2. Gaussian beam at eigenfrequency of $N+m$=40 reveals the trajectories of light rays of our design in geometrical optics, see Fig. 2(e). In Fig. 2(f), we also use plane wave at eigenfrequency of $N+m$=10 to show almost perfect transparency effect in wave regime. All numerical full wave simulations in this paper are calculated by the commercial software COMSOL MULTIPHYSICS.

The main property of our design based on geodesic lenses is that the resulting refractive index profile is a continuous scalar field. We could carefully design virtual space to achieve more feasible parameters. For the design of conformal transparency, we should take care of two things. One is that the branch cut should be geodesic of both surfaces in virtual space. Otherwise, light rays would have a chance to cross the branch cut immediately once they have left it, which would compromise the effect of transparency. The other thing is that the length of the branch cut should not be larger than half of a great circle. Otherwise, some light rays entering the sphere through the branch cut could leave the sphere before completing the closed loop on it, which would also compromise the effect of transparency. Recently, by setting the length of branch cut half of the great circle, conformal transparency with an optimized refractive index profile ranging from 0 to 5.21 was achieved [26].

5. Other designs based on geodesic lenses

5.1. Another design of conformal transparency

Suppose that we have a virtual space combined with a plane and a truncated Tannery's pear shown in Fig. 3(a), which are connected along with a branch cut (a line in purple). The branch cut on both surfaces is also part of a geodesic. Parallel light rays shown in colored curves propagate in the plane and meet the branch cut, they enter the truncated Tannery's pear and form closed trajectories which have been mentioned above. Then they come back to the branch cut and return into the plane to continue their journey with their positions and directions preserved. But for an observer far away from the truncated Tannery's pear, it appears invisible within geometrical optics.

Based on this virtual space, we could use a geodesic mapping from the truncated Tannery's pear to an inverse invisible lens in Fig. 3(b). Then by further using Zhukowski conformal mapping, namely $w = z + 1/z$ [2], the whole virtual space in Fig. 3(b) is mapped to a physical space in Fig. 3(c), which has a continuous refractive index profile ranging from 0 to 16.

This design of conformal transparency is a composition of a geodesic mapping and a Zhukowski mapping. Owing to that truncated Tannery's pear is also a geodesic lens, its

Optics EXPRESS

spectrum is approximately $\omega r_0 / c \approx N + m + 0.5$ from the numeric method [39], which is listed in Table 1. We also use numerical simulation to demonstrate the performance of our design with r_0=2 , see Fig. 3(d) with Gaussian beam by setting $N + m$=20 and Fig. 3(e) with the plane wave by setting $N + m$=6 to demonstrate the geometric-optical regime and wave-optical regime, respectively.

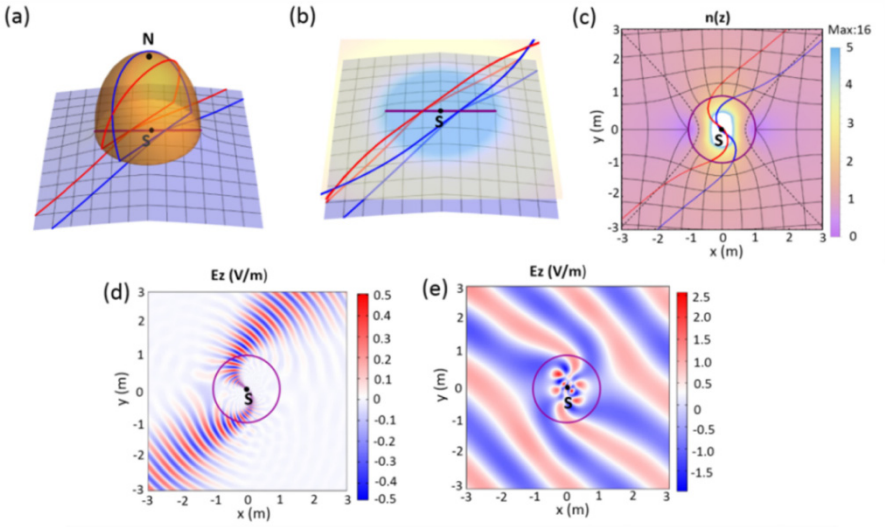

Fig. 3. Another conformal transparency design based on a truncated Tannery's pear. Virtual space (a) consists of a complex plane and a truncated Tannery's pear. They are sewed along with a branch cut (solid line in purple), which belongs to geodesics of both parts, namely a straight line of the plane and a straight line of the truncated Tannery's pear. Its length is 4. Two colored light rays (in red and in blue) are paralleled in plane and form closed trajectories in truncated Tannery's pear. Using geodesic mapping, truncated Tannery's pear in (a) is mapped to inverse invisible lens in (b). Using a Zhukowski mapping, (b) is further mapped to physical space in (c), where dashed black lines are places with the refractive index of unity. Corresponding light rays (in red and in blue) are shown in colored curves in (a-d). Gaussian beam in (d) and plane wave in (e) impinge our design at the angle of π/4 at eigenfrequency with $N + m$=20 and $N + m$=6, respectively. Here we set the length of the branch cut to be 4 for the illustration.

5.2. Wave reflection

Besides optical conformal transparency, we could also achieve wave omnidirectional reflection, which looks like a double-sided mirror from the outside. We start with virtual space, which is a combination of a plane and spindle surface shown in Fig. 4(a). They are sewed along with a branch cut (an arc in purple). The branch cut is geodesic of both parts, namely it belongs to the straight line of the plane and the equator of spindle surface. Parallel light rays shown in colored curves propagate initially in the plane. Those of them that cross the branch cut enter the spindle surface, travel along closed trajectories, and come back to the branch cut with their positions preserved but directions reflected. For observers far away from spindle surface, light rays seem to be totally reflected from the branch cut.

After performing geodesic mapping and exponential analytical conformal mapping, the spindle surface is mapped to Mikealian lens with a period of 16π shown in Fig. 4(b). The period here is twice larger than that in conformal transparency design. By carefully choosing an analytical conformal mapping which is written as $w_1 = z + 4\log(z-a) - 4\log(z+a)$, we map the whole structure to physical space in Fig. 4(c) with a contour plot of refractive index profile. The analytical conformal mapping here has a slight difference from that in conformal transparency design. It can be even chosen such that the branch cut could be the whole circle

Optics EXPRESS

of the spindle. In Fig. 4(d), we also perform a numeric simulation to demonstrate wave reflection with Gaussian beam by setting $N+m$=30. The conformal reflection works perfectly at any frequency, not just the resonant ones of conformal transparency in wave optical regime.

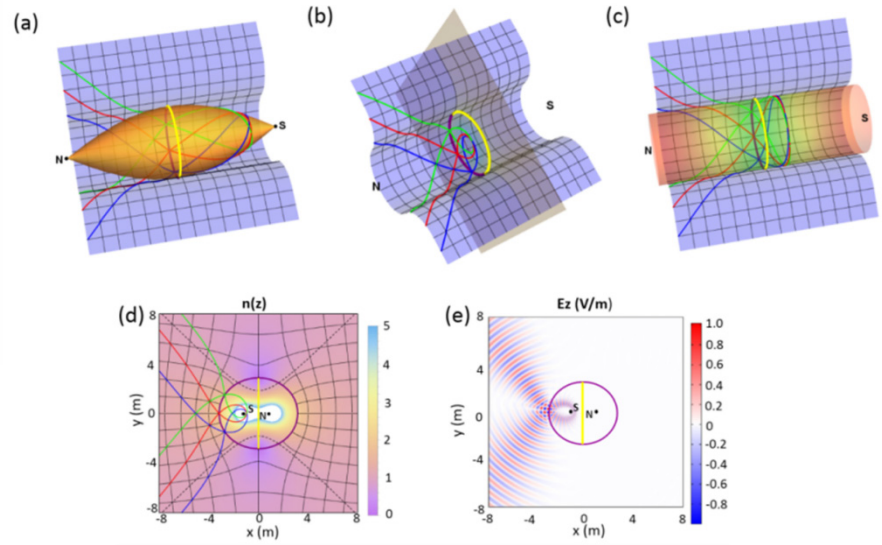

Fig. 4. Conformal reflection design based on a spindle. Virtual space (a) consists of a complex plane and a spindle. They are sewed along with a branch cut (solid arc in purple), which belongs to geodesics of both parts, namely a straight line of the plane and the equator of the spindle. Using geodesic mapping, the spindle is mapped to a generalized Maxwell's fish-eye lens in (b). With a further exponential conformal mapping, Maxwell's fish-eye lens in (b) is mapped to a cylindrical Mikealian lens shown in (c). Using an analytical conformal mapping, physical space is finally obtained in (d), with the contour plot of refractive index profile (Dashed black lines are places with the refractive index of unity). Corresponding light rays are shown in colored curves in (a-d). Gaussian beam in (e) impinges our design at the angle of $-\pi/4$ with a frequency corresponding to $N+m$=30. For the illustration, the length of the equator and the branch cut are set to be 4π and 12.14, respectively. The corresponding parameter a in an analytical conformal mapping is 1.2.

5.3. Two methods for achieving invisibility cloaks

Based on the above designs, we can further achieve invisible cloaks with two methods. One is that we employ the fact that there is some place in the virtual space, where light rays coming from the outside could not reach, such as the two yellow curves in Fig. 2(a). These two yellow curves could be equipped with PECs. This way, we can naturally achieve invisible cloaks using PECs. This method is similar to that used in non-Euclidean cloaks [43]. The other method is that we can place a PEC along a meridian of the geodesic lens as shown in black closed curve of Figs. 5(a), 5(c) and 5(e) to reflect light rays twice, which will give an invisible cloak as well [26]. The PEC divides the branch cut into two equal parts. As shown in Figs. 5(b), 5(d) and 5(f), it seems that these PECs in black lines are invisible, similar to that in Figs. 2(f), 3(e) and 4(d), respectively. We call this method "double-reflection mechanism". Once we make the PEC invisible, we can further expand it to make cloaking region of cloaking by another conformal mapping [46].

Optics EXPRESS

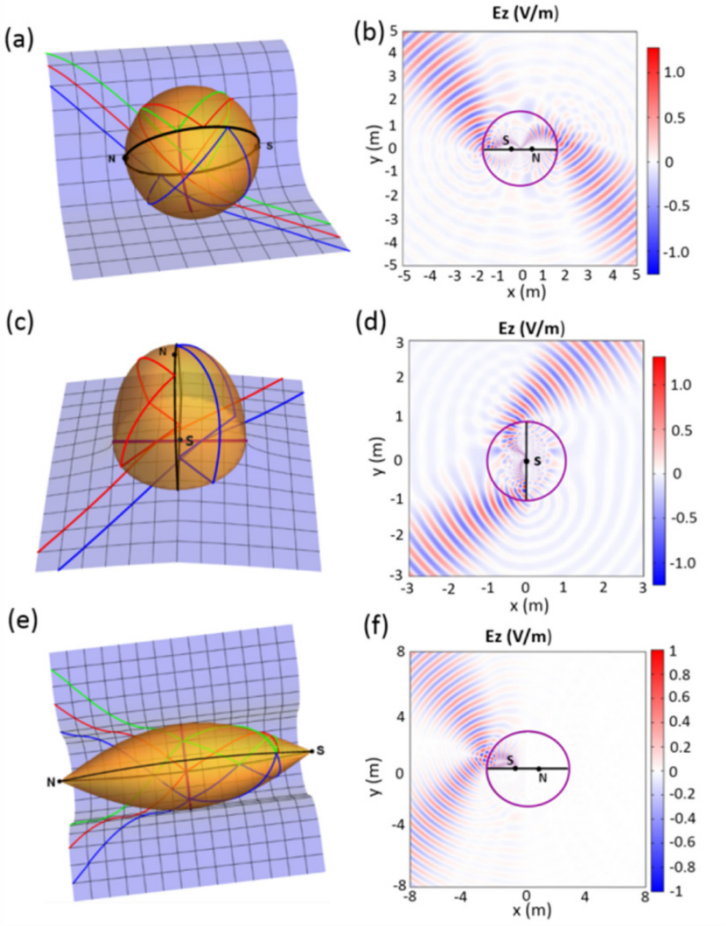

Fig. 5. Invisibility cloaks of PECs. PECs (in black) along closed geodesics of geodesic lenses of Figs. 2(a), 3(a) and 4(a), are located to divide the branch cut into equal parts. Once light rays meet the PECs, they are reflected. Light rays are shown in colored curves in (a), (c) and (e). Gaussian beams in (b), (d) and (f) are consistent with trajectories of light rays at the same condition of corresponding physical spaces of Figs. 2(e), 3(d) and 4(e).

In the first design of the above conformal transparency, we can use another PEC, which gives the double-reflection mechanism as well. One such PEC is a great circle of the sphere in black as shown in Fig. 6(a). This PEC touches one vertex of the branch cut. After light rays enter the sphere, they will be reflected by the PEC twice and form closed trajectories. Therefore light rays will never reach the other half of the sphere because of the PEC. After mapping virtual space to physical space as in Fig. 6(b), we obtain a cloaking region bounded by the PEC in black. We can also modify our device by removing a part of the PEC as is shown in Figs. 6(c) and 6(d) or, alternatively, Figs. 6(e) and 6(f). In this case, the remaining PEC will reflect light rays twice and the sphere will still be invisible, but the cloaked region will be lost.

Optics EXPRESS

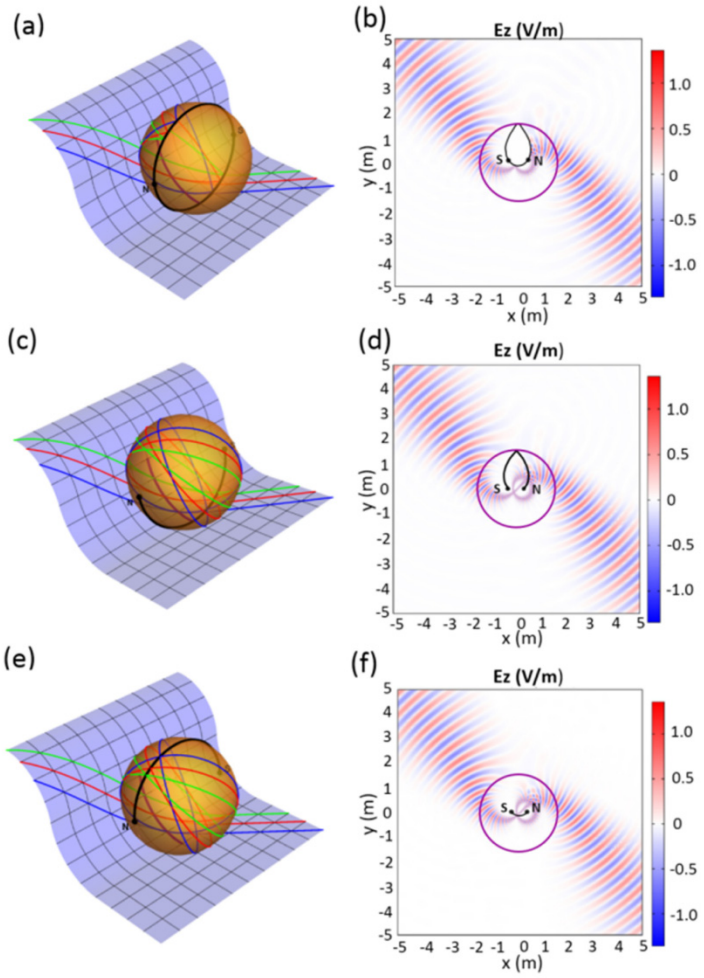

Fig. 6. Conformal cloaks of PECs. (a) PECs (in black) along with the closed geodesic of the sphere of Fig. 2(a) is located to pass through one vertex of the branch cut, N and S poles. Double reflection on this PEC could make half of the sphere invisible. (b) This way, a waterdrop-shape cloaking region is obtained in physical space. In fact, both halves of this PEC, which connects N and S pole, are invisible by double-reflection mechanism as shown in (c) and (e), respectively. Light rays are shown in colored curves in (a), (c) and (e). Propagation of a Gaussian beam with the same parameters as in Fig. 2(e), as shown in (b), (d) and (f).

6. Conclusion

In conclusion, we propose a special method of conformal transformation optics based on geodesic lenses. The resulting refractive index profile is a continuous refractive index profile and shows the almost perfect performance of the designed devices. We demonstrate our method by achieving optical transparency and wave reflection. Furthermore, we can achieve invisible cloaks with two methods. Thanks to the intuition of virtual space, we further explain the mechanism of conformal transparency at eigenfrequencies in wave optics. Such a method may also find applications in other dynamic waves.

Funding

National Science Foundation of Anhui Province of China (1908085QA20); Czech Science Foundation (P201/12/G028); National Natural Science Foundation of China (NSFC)

Optics EXPRESS

(11874311 and 11904006); Fundamental Research Funds for the Central Universities (20720170015).

References

1. E. J. Post, *Formal Structure Of Electromagnetics: General Covariance and Electromagnetics* (Courier Corporation, 1997).
2. U. Leonhardt, "Optical conformal mapping," Science **312**(5781), 1777–1780 (2006).
3. J. B. Pendry, D. Schurig, and D. R. Smith, "Controlling electromagnetic fields," Science **312**(5781), 1780–1782 (2006).
4. U. Leonhardt and T. G. Philbin, "General relativity in electrical engineering," New J. Phys. **8**(10), 247 (2006).
5. H. Chen, C. T. Chan, and P. Sheng, "Transformation optics and metamaterials," Nat. Mater. **9**(5), 387–396 (2010).
6. A. V. Kildishev and V. M. Shalaev, "Transformation optics and metamaterials," Phys. Uspekhi **54**(1), 53–63 (2011).
7. P. Kinsler and M. W. McCall, "The futures of transformations and metamaterials," Photon. Nanostructures **15**, 10–23 (2015).
8. J. Li and J. B. Pendry, "Hiding under the carpet: a new strategy for cloaking," Phys. Rev. Lett. **101**(20), 203901 (2008).
9. Y. Lai, J. Ng, H. Chen, D. Han, J. Xiao, Z.-Q. Zhang, and C. T. Chan, "Illusion optics: the optical transformation of an object into another object," Phys. Rev. Lett. **102**(25), 253902 (2009).
10. H. Chen and C. Chan, "Transformation media that rotate electromagnetic fields," Appl. Phys. Lett. **90**(24), 241105 (2007).
11. D. Schurig, J. J. Mock, B. J. Justice, S. A. Cummer, J. B. Pendry, A. F. Starr, and D. R. Smith, "Metamaterial electromagnetic cloak at microwave frequencies," Science **314**(5801), 977–980 (2006).
12. R. Liu, C. Ji, J. J. Mock, J. Y. Chin, T. J. Cui, and D. R. Smith, "Broadband ground-plane cloak," Science **323**(5912), 366–369 (2009).
13. H. F. Ma and T. J. Cui, "Three-dimensional broadband ground-plane cloak made of metamaterials," Nat. Commun. **1**(1), 21 (2010).
14. H. Chen, B. Hou, S. Chen, X. Ao, W. Wen, and C. T. Chan, "Design and experimental realization of a broadband transformation media field rotator at microwave frequencies," Phys. Rev. Lett. **102**(18), 183903 (2009).
15. M. M. Sadeghi, S. Li, L. Xu, B. Hou, and H. Chen, "Transformation optics with Fabry-Pérot resonances," Sci. Rep. **5**(1), 8680 (2015).
16. J. Luo, Y. Yang, Z. Yao, W. Lu, B. Hou, Z. H. Hang, C. T. Chan, and Y. Lai, "Ultratransparent Media and Transformation Optics with Shifted Spatial Dispersions," Phys. Rev. Lett. **117**(22), 223901 (2016).
17. S. Viaene, V. Ginis, J. Danckaert, and P. Tassin, "Transforming two-dimensional guided light using nonmagnetic metamaterial waveguides," Phys. Rev. B **93**(8), 085429 (2016).
18. C. Sheng, H. Liu, Y. Wang, S. Zhu, and D. Genov, "Trapping light by mimicking gravitational lensing," Nat. Photonics **7**(11), 902–906 (2013).
19. C. Sheng, R. Bekenstein, H. Liu, S. Zhu, and M. Segev, "Wavefront shaping through emulated curved space in waveguide settings," Nat. Commun. **7**(1), 10747 (2016).
20. H. Chen and C. T. Chan, "Acoustic cloaking and transformation acoustics," J. Phys. D Appl. Phys. **43**(11), 113001 (2010).
21. Y. Liu, T. Zentgraf, G. Bartal, and X. Zhang, "Transformational plasmon optics," Nano Lett. **10**(6), 1991–1997 (2010).
22. C. Fan, Y. Gao, and J. Huang, "Shaped graded materials with an apparent negative thermal conductivity," Appl. Phys. Lett. **92**(25), 251907 (2008).
23. H. Li, Y. Xu, and H. Chen, "Conformal cloaks at eigenfrequencies," J. Phys. D Appl. Phys. **46**(13), 135109 (2013).
24. Q. Wu, Y. Xu, H. Li, and H. Chen, "Cloaking and imaging at the same time," Europhys. Lett. **101**(3), 34004 (2013).
25. L. Xu and H. Chen, "Logarithm conformal mapping brings the cloaking effect," Sci. Rep. **4**(1), 6862 (2014).
26. L. Xu, H. Chen, T. Tyc, Y. Xie, and S. A. Cummer, "Perfect conformal invisible device with feasible refractive indexes," Phys. Rev. B **93**(4), 041406 (2016).
27. Z. Xiong, L. Xu, Y.-D. Xu, and H.-Y. Chen, "Broadband illusion optical devices based on conformal mappings," Front. Phys. **12**(5), 124202 (2017).
28. X. Wang, H. Chen, H. Liu, L. Xu, C. Sheng, and S. Zhu, "Self-focusing and the Talbot effect in conformal transformation optics," Phys. Rev. Lett. **119**(3), 033902 (2017).
29. Y. Liu, F. Sun, and S. He, "Controlling lightwave in Riemann space by merging geometrical optics with transformation optics," Sci. Rep. **8**(1), 514 (2018).
30. C. Gu, K. Yao, W. Lu, Y. Lai, H. Chen, B. Hou, and X. Jiang, "Experimental realization of a broadband conformal mapping lens for directional emission," Appl. Phys. Lett. **100**(26), 261907 (2012).
31. Y. Ma, Y. Liu, L. Lan, T. Wu, W. Jiang, C. K. Ong, and S. He, "First experimental demonstration of an isotropic electromagnetic cloak with strict conformal mapping," Sci. Rep. **3**(1), 2182 (2013).

Optics EXPRESS

32. L. Xu and H. Chen, "Conformal transformation optics," Nat. Photonics **9**(1), 15–23 (2015).
33. M. Šarbort and T. Tyc, "Spherical media and geodesic lenses in geometrical optics," J. Opt. **14**(7), 075705 (2012).
34. M. Šarbort, *Non-Euclidean Geometry in Optics* (Masaryk University, 2013).
35. G. C. Righini, V. Russo, S. Sattini, and G. T. Francia, "Thin film geodesic lens," Appl. Opt. **11**(6), 1442–1443 (1972).
36. G. C. Righini, V. Russo, S. Sottini, and G. T. di Francia, "Geodesic lenses for guided optical waves," Appl. Opt. **12**(7), 1477–1481 (1973).
37. Z. Nehari, *Conformal Mapping* (McGraw-Hill Book Company, 1952)
38. U. Leonhardt and T. Philbin, *Geometry and Light: The Science of Invisibility* (Dover, 2010).
39. L. Xu, X. Wang, T. Tyc, C. Sheng, S. Zhu, H. Liu, and H. Chen, "Light rays and waves on geodesic lenses," arXiv:1801.10438 (2018).
40. A. L. Besse, *Manifolds All of Whose Geodesics Are Closed* (Springer Science & Business Media, 2012).
41. T. Needham, *Visual Complex Analysis* (Oxford University, 1998).
42. T. Tyc, L. Herzánová, M. Šarbort, and K. Bering, "Absolute instruments and perfect imaging in geometrical optics," New J. Phys. **13**(11), 115004 (2011).
43. U. Leonhardt and T. Tyc, "Broadband invisibility by non-Euclidean cloaking," Science **323**(5910), 110–112 (2009).
44. H. Chen, U. Leonhardt, and T. Tyc, "Conformal cloak for waves," Phys. Rev. A **83**(5), 055801 (2011).
45. T. Tyc and A. J. Danner, "Absolute optical instruments, classical superintegrability, and separability of the Hamilton-Jacobi equation," Phys Rev. A. **96**(5), 053838 (2017).
46. T. Tyc, H. Chen, C. T. Chan, and U. Leonhardt, "Non-Euclidean cloaking for light waves," IEEE J. Sel. Top. Quantum Electron. **16**(2), 418–426 (2010).
47. L. Xu, Z. Xiong, and H. Chen, "Analysis of a conformal invisible device," Front. Phys. **13**(2), 134203 (2018).
48. H. Kan, L. Xu, Y. Xu, and H. Chen, "Conformal cloaks from a function composition," Europhys. Lett. **117**(3), 34002 (2017).